Chinese Chemical Letters 36 (2025) 109600

Contents lists available at ScienceDirect

Chinese Chemical Letters

journal homepage: www.elsevier.com/locate/cclet

Co^{II} single-ion magnet and its multi-dimensional aggregations: Influence of the structural rigidity on magnetic relaxation process

Zhao-Bo Hu[a,b,f,*], Ling-Ao Gui[a], Long-He Li[a], Tong-Tong Xiao[c], Adam T. Hand[d], Pagnareach Tin[d], Mykhaylo Ozerov[e], Yan Peng[a,f], Zhongwen Ouyang[c], Zhenxing Wang[c], Zi-Ling Xue[d,*], You Song[b,*]

[a] Chaotic Matter Science Research Center, Faculty of Materials Metallurgy and Chemistry, Jiangxi University of Science and Technology, Ganzhou 341000, China
[b] State Key Laboratory of Coordination Chemistry, School of Chemistry and Chemical Engineering, Nanjing University, Nanjing 210023, China
[c] Wuhan National High Magnetic Field Center & School of Physics, Huazhong University of Science and Technology, Wuhan 430074, China
[d] Department of Chemistry, University of Tennessee, Knoxville, TN 37996, United States
[e] National High Magnetic Field Laboratory, Florida State University, Tallahassee 32310, United States
[f] Jiangxi Provincial Key Laboratory of Functional Molecular Materials Chemistry, Jiangxi University of Science and Technology, Ganzhou 341000, China

ARTICLE INFO

Article history:
Received 20 December 2023
Revised 21 January 2024
Accepted 29 January 2024
Available online 4 February 2024

Keywords:
Spin-phonon coupling
Slow magnetic relaxation
Structural rigidity
Co^{II} compounds
Far-IR magneto-spectra

ABSTRACT

Two Co^{II}-based complexes, $\{[Co(dps)_2(N_3)_2]\cdot H_2O\}_n$ (**1**) and $[Co(dps)_2(N_3)_2]_n$ (**2**), show a 1D chain and a 3D network, respectively. The central Co^{II} ions in the complexes have the same coordination environment with the $[Co(dps)_4(N_3)_2]$ unit. Although the differences in crystal parameters are nearly negligible, their magnetic properties are very different. AC susceptibility data show that **1** behaves as a typical field-induced single-ion magnet (SIM) with the out-of-phase (χ_M") signals, while **2** shows ac signals of χ_M" without peaks even under applied dc filed within our measurement window. Far-IR magneto-spectra (FIRMS) show strong spin-phonon couplings at 0 T in **2**, likely making the magnetic relaxation in **2** fast, while the couplings are negligible in **1.** Small spin-phonon coupling in **1** likely leads to slower magnetic relaxation, making **1** a SIM. The difference in the properties is due to the structural rigidity of **2** in its 3D network, leading to stronger spin-phonon coupling. Combined high-field EPR (HF-EPR) and FIRMS studies give spin-Hamiltonian parameters, including $D = 64.0(9)$ cm^{-1}, $|E| = 15.7(2)$ cm^{-1} for **1** and $D = 80.0(2)$ cm^{-1}, $|E| = 19.0(1)$ cm^{-1} for **2**.

Single-molecule magnets (SMMs) have been a hot topic due to their potential applications in spintronics and quantum computers [1–7]. Single-ion magnets (SIMs) are a special kind of SMMs with one metal ion in molecules [8–11] and intensely studied [12–27]. Highly axial structures and ligand-field tuning can increase magnetic anisotropy, improving effective energy barriers and blocking temperatures of SIMs [14–26]. However, no breakthrough has been made since the record blocking temperature by $[(Cp^iPr_5)Dy(Cp^*)]^+$ was attained [19,20].

In Layfield's work, it is found that not only the structural symmetry plays an important role in the SIM performance but also the molecular vibration has an impact on the effective energy barrier and blocking temperature [19,24,28]. Recently, Sessoli's group proved that spin-phonon coupling plays a crucial role in the spin relaxation process of a mononuclear complex, providing a theoretical basis for the design and synthesis of high-performance SIMs [27]. In our early work, we also found that the effect of isotopic vibration on the slow relaxation process by comparing CH_3CN and CD_3CN [29]. However, in most cases, especially in coupled systems, the spin-phonon coupling could not be observed because the magnetic coupling is much stronger [30–33]. Therefore, this effect has not attracted much attention and was often ignored when the coupling between spin carriers is mainly considered, although experimental observations of spin-phonon couplings have been reported in recent years [34–40]. Spin-phonon coupling is rarely considered in the design and synthesis of molecular magnets due to unpredictability of this property.

To prove the existence and importance of spin-phonon coupling in molecular magnets, we have designed two complexes with the same coordination environment and negligible magnetic exchange between adjacent metals, but different structural dimen-

* Corresponding authors.
E-mail addresses: huzhaobo@smail.nju.edu.cn (Z.-B. Hu), xue@utk.edu (Z.-L. Xue), yousong@nju.edu.cn (Y. Song).

https://doi.org/10.1016/j.cclet.2024.109600
1001-8417/

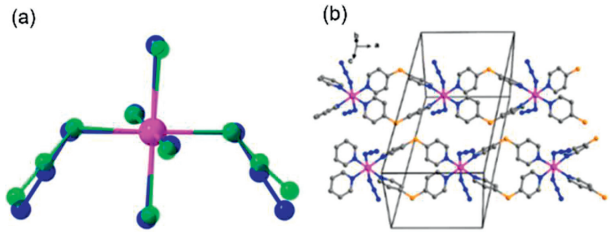

Fig. 1. (a) Coordination environment of Co^{II} ions in **1** and **2**. Blue atoms represent atoms in **1** and green atoms represent those in **2**. (b) Stacking diagram in a cell frame of **1**.

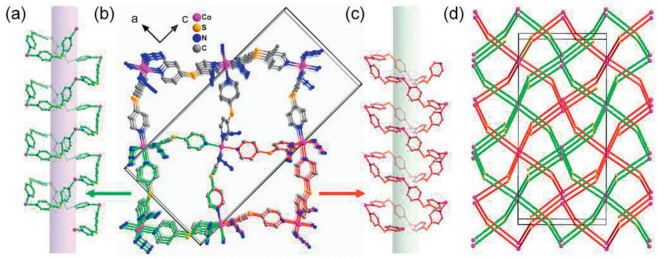

Fig. 2. Stacking diagram in a cell frame of **2**: (a-c) Mirror-symmetric chiral channels within the racemate framework of **2**. (d) Topological views of **2**. Pink = Co, Yellow = dps.

sionalities. The effect of spin-phonon interaction on the relaxation process has been probed experimentally. The two complexes are composed of the same $[Co(dps)_4(N_3)_2]$ unit, but show one- and three-dimensions (1D and 3D), respectively. There is no measurable magnetic exchange between the Co^{II} centers in each complex, helping study the vibrational effects on slow magnetic relaxation. AC susceptibility data shows that they are both field-induced SIMs. FIRMS spectra show strong spin-phonon coupling in **2** most likely from its 3D lattice rigidity, leading to its weaker SIM property than **1** (with a 1D structure). The results demonstrate the influence of spin-phonon coupling on magnetic relaxation. Herein, we report structures of **1** and **2**, their magnetic properties and the magnetostructural correlation based on HF-EPR and FIRMS results.

The structure of **1** has been reported [41]. Both complexes have the similar structural unit of $[Co(dps)_4(N_3)_2]$. The difference is in the numbers of solvent water molecules in the lattices, leading to the 1D chain and 3D framework of **1** and **2** with a monoclinic and orthorhombic space group, respectively. In order to ensure the purity of both complexes, PXRD and IR were measured for **1** and **2** (Figs. S1 and S2 in Supporting information). The results prove that both complexes are pure phases.

In **1**, one unit contains one Co^{II} ion, four dps molecules, two N_3^- anions and one lattice water molecule (Fig. S3 in Supporting information). The surrounding metal center Co^{II} ion shows a hexacoordinate octahedral geometry (Fig. 1a). Among the six N atoms involved in the coordination, four of them are from the ligand dsp and the other two are from N_3^-. The non-coplanar pyridine rings destroy the conjugation of the bridging ligand, which cannot effectively mediate the coupling between spins. The lengths of Co-N(N_3^-) bonds are 2.066(8) and 2.097(7) Å, which are shorter than other Co-N bonds. Thus, the coordination configuration of Co^{II} ion can be regarded as a compressed octahedron. These two opposite coordinated N atoms and Co^{II} ion are almost collinear. The N-Co-N bond angles are 176.16°, 176.20° and 177.48°, respectively. The nearest Co^{II} ions are linked together by two dps ligands to form a 1D chain along the a-axis, in which each of the two dps ligands provides two pyridine groups to bridge two adjacent metal ions (Fig. 1b). The expanded structure is stabilized by the very weak interaction from the sulfur atom of the dps ligand to the pyridine group in the neighboring chain (the shortest S···C distance is 3.383 Å) and the hydrogen bond provided by lattice water between chains.

The asymmetric unit of complex **2** is very similar to that of **1**. The center Co^{II} ions also adopt a distorted compressed octahedral coordination geometry, in which the Co-N(N_3^-) bond lengths of 2.090(3) and 2.098(3) Å are slightly less than that of the Co-N(dps) bond. A main structural difference between **2** and **1** is its 2-fold interpenetrated 3D framework (Figs. 2a-c), which depends on the arrangement of dps ligands around one Co^{II} center. In **1**, two dps ligands bridge two Co^{II} ions and four Co-N coordination bonds are coplanar with two S atoms in different ligands. This type of double bridging results in an approximately square closed Co-$(dps)_2$-Co ring, which is repeated to constitute the chain structure of **1**. In contrast, Co^{II} ions in **2** are linked by a single dps bridge. Every four Co^{II} ions and four ligands bridging among them act as a repeating helical unit, giving an approximately square helical channel (Figs. 2a and c). Within the helical chain, the Co···Co distance is 11.557 Å, equivalent to the side length of a square channel. The screw pitch of a helical channel is the distance between two adjacent Co ions, *i.e.*, 9.524 Å. Because one Co^{II} ion is coordinated by four dps ligands in the equatorial plane, there are four helical channels with the Co^{II} ion as a 4-connected node (Fig. 2d). The adjacent channels have opposite chirality. Thus, each framework structure is a racemate. In **2**, there are two sets of completely equivalent frameworks that are interspersed with each other, leading to the 2-fold interpenetration in a translation fashion (Fig. 2d). The crystal structure of **2** is stabilized by van der Waals forces, resulting in a dense framework without accessible porosity. Since **1** and **2** have similar local coordination environments (Fig. 1a), the difference between them is only in the dimensionality of 1D and 3D. These structural characteristics will help understand the role of spin-phonon coupling in the relaxation in **1** and **2**.

Both complexes exhibit similar $\chi_M T$ values of 3.12 cm^3 K/mol for **1** and 3.14 cm^3 K/mol for **2** at room temperature, respectively (Fig. 3). The larger than the spin-only value of 1.875 cm^3 K/mol for an isolated high spin Co^{II} complex (assuming $S = 3/2$ and $g = 2.0$) is commonly associated with the orbital contribution through the spin-orbit coupling. With the lowering of temperature, the $\chi_M T$ values first gradually decrease from room temperature to 150 K, and then show a more pronounced decrease, finally reaching ultimate values of 1.93 cm^3 K/mol for **1** and 1.86 cm^3 K/mol for **2**, respectively, at 1.8 K. This behavior is commonly associated with the depopulation of Kramers' excited states ($M_s = \pm 1/2$ and $\pm 3/2$). The field-dependence of the magnetization for **1** and **2** were measured in fields ranging from 0 to 70 kOe at temperature varies between 1.8 and 10.0 K (insert in Fig. 3). The magnetization reaches 2.32 $N\mu_B$ for **1** and 2.27 $N\mu_B$ for **2** at 70 kOe, respectively, but does not saturate as it is expected for an anisotropic ion. The temperature- and field-dependent mgnetization data of **1** and **2** were fitted using the PHI program to quantify the anisotropy parameters [42]. Good fits were obtained using the following spin-Hamiltonian (SH):

$$\hat{H} = D\left[\hat{S}_z^2 - \frac{S(S+1)}{3}\right] + E\left(\hat{S}_x^2 - \hat{S}_y^2\right) + g\mu_B SH \quad (1)$$

The best fits of the reduced magnetization data give $D = 62.26(22)$ cm^{-1}, $E = 10.76(10)$ cm^{-1} ($E/D = 0.17$), $g_x = g_y = 2.65(9)$, $g_z = 2.41(6)$ and $TIP = 1.13 \times 10^{-4}$ cm^3/mol for **1** and $D = 74.94(15)$ cm^{-1}, $E = 19.06(19)$ cm^{-1} ($E/D = 0.25$), $g_x = g_y = 2.61(10)$, $g_z = 2.38(10)$ and $TIP = 1.13 \times 10^{-4}$ cm^3/mol for **2**. These SH parameters were obtained using fitting procedure in PHI software [42] and SH parameters from HFEPR analysis as a starting point.

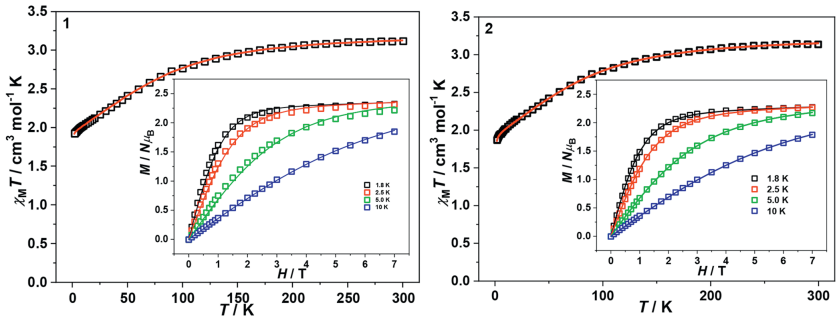

Fig. 3. Temperature dependence of $\chi_M T$ for **1** and **2**. Insert: Isothermal magnetization at different temperatures for **1** and **2**. The solid line is the best fitting result.

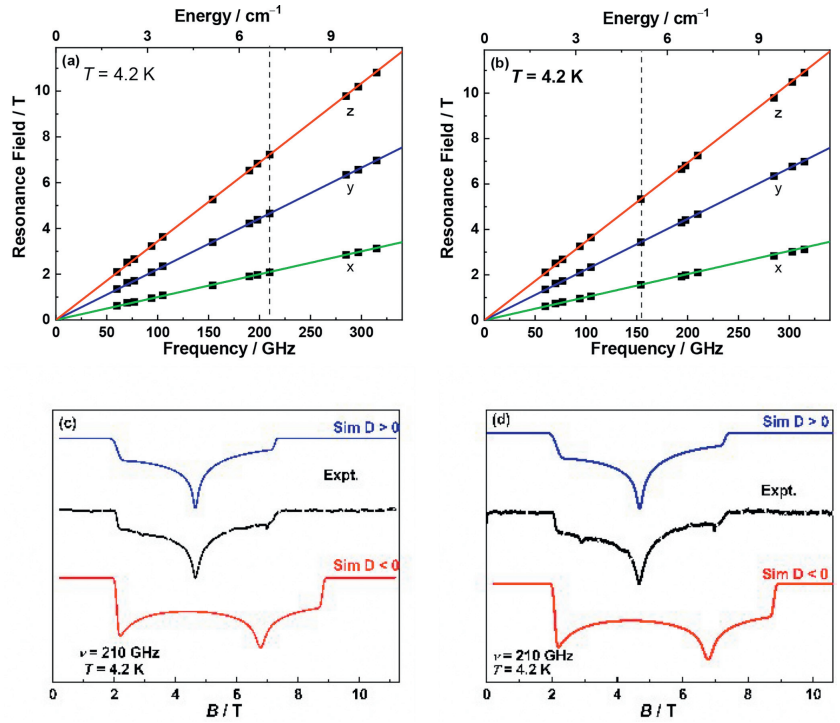

Fig. 4. (a, b) Resonance field *vs.* microwave frequency for EPR transitions, and (c, d) HF-EPR spectra with simulations at 4.2 K of **1** and **2**. Green, blue, and red curves are the simulations using the best-fitted spin-Hamiltonian parameters with the magnetic field H parallel to the x, y, and z axes of the ZFS tensor, respectively. The vertical dashed line represents the frequency used at which the spectra were recorded or simulated.

To get more details on the SH model of **1** and **2**, HF-EPR measurements were performed in the frequency range of 60–375 GHz (Fig. 4 and Fig. S4 in Supporting information). The HF-EPR spectra of **1** and **2** contain three main components arising from the intra-Kramers transitions within the lowest doublet $M_S = \pm 1/2$ with $\Delta M_S = \pm 1$. These features indicate that two complexes are typically $S = 3/2$ systems with large, positive D values. Simulations of the HF-EPR spectra are made using the $|D|$ values from FIRMS below, while adjusting E and g values *via* SPIN [43]. The best simulated spectra were obtained with the following parameters: $D = 64.0(9)$ cm^{-1}, $|E| = 15.7(2)$ cm^{-1} ($|E/D| = 0.245$), $g_x = g_y = 2.62(2)$, $g_z = 2.45(2)$ for **1** and $D = 80.0(3)$ cm^{-1}, $|E| = 19.0(1)$ cm^{-1} ($|E/D| = 0.236$), $g_x = g_y = 2.58(2)$, and $g_z = 2.42(2)$ for **2**. The simulations of the HF-EPR spectra indicate the positive sign of D value (Fig. 4, bottom), suggesting the easy-plane anisotropy for both **1** and **2**.

FIRMS is a powerful tool to directly determine the large ZFS in transition metal complexes [44–47]. The combined use of FIRMS and EPR has been adopted recently to give accurate SH parameters [46–50]. Also, FIRMS allows to observe the spin-phonon coupling effect [34–39].

The transmission spectra (Figs. 5a and b) were measured for powder samples at the temperature of 5.5 K, and at fixed magnetic field varied between 0 and 17.5 T with step of 0.5 T. To distinguish inter-KD transitions from the non-magnetic phonon peaks, all spectra were normalized to the reference spectrum, which is calculated as an average spectrum for all magnetic fields. Figs. 5c and d show the heatmap of such normalized transmittance with blue color corresponding to the intensive ZFS transitions, while yellow indicate transmission unaffected by magnetic fields. The ZFS energy ($2D$') is evaluated as 139(2) cm^{-1} for **1** and 172(5) cm^{-1} for **2** from zero-field slice of the heat map, respectively.

Spin-phonon coupling in **2** can also be observed by comparing the FIRMS heatmap with those of **1**. For **1** (Figs. 5a and c), no significant spin-phonon coupling is observed at 0 T. When the external magnetic field is applied, the magnetic transitions shift as a result of Zeeman effect. Between 6 T and 10 T, avoided-crossings between the blue-shifting magnetic transitions and phonon peaks are observed in Fig. 5c. However, a comparison of the far-IR spectra at 0 and 17.5 T in Fig. 5a shows small overall differences, indicating weak (or negligible) spin-phonon coupling in **1** at 0 T. In

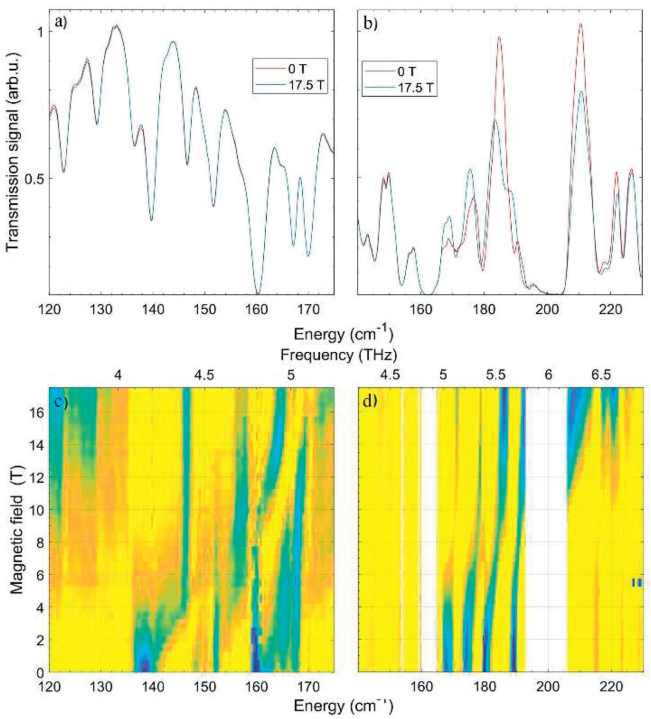

Fig. 5. FIRMS spectra of (a) **1** and (b) **2**. The top panel shows transmission spectra at 0 and 17.5 T. Vertical stripes at the phonon peaks (a) and (b) are distortions due to the spin-phonon coupling in **2**. Normalized 2D plots revealing ZFS values $2D' = 139(2)$ cm^{-1} for (c) **1** and 172(5) cm^{-1} for (d) **2**.

contrast, for **2** (Figs. 5b and d), spin-phonon coupling is prominent even at 0 T (without the external magnetic field), leading to a few spin-phonon coupled states. The far-IR spectra of **2** at 0 and 17.5 T (Fig. 5b) show significant differences near the magnetic transition at 172(5) cm^{-1}. The strong spin-phonon coupling in **2** may make its magnetic relaxation fast. The difference in FIRMS between **1** and **2** is consistent with the AC susceptibility data below that **1** is a SIM, while **2** is not.

The temporal behavior of magnetization for **1** and **2** was investigated by two types of experiments. First, the ac-susceptibilities were measured as a function of frequencies at one temperature and in different applied fields from 0 to 3.0 kOe. Second, their frequency dependences were measured at a fixed bias dc-magnetic field for different temperatures from 1.8 K to 7.0 K. The measurements were performed on polycrystalline samples using a VSM magnetometer. The first observation was that the out-of-phase ac-susceptibility (χ_M") for **1** and **2** has no signal in zero field but is clearly enhanced in 1 kOe (Fig. S5 in Supporting information). Such behavior has been associated with the presence of QTM. This result indicates that each Co^{II} molecule in **1** and **2** behaves as a SIM. To explore the magneto-structural correlation, 1.5 kOe for **1** was chosen to measure the dynamic magnetization due to the longest relaxation time.

In the given field and temperature ranges, the variable-frequency χ_M" for **1** are shown in Fig. 6. The Cole-Cole plots of χ_M" *vs.* χ_M' for **1** were fitted using the CC-FIT program and a modified Debye function (Fig. S6 in Supporting information) [51]. The relaxation times τ_0 and effective barrier energies were obtained from fitting the Arrhenius-like diagrams (Fig. S7 in Supporting information). The whole temperature data set was fitted to Eq. 2 containing three relaxation processes, where A represents direct process, B is the coefficient of the Raman process, U_{eff} is the energy barrier for magnetization reversal, k_B is the Boltzmann constant, and T is temperature. The best fitting parameters are $A = 60.76\,K^{-1}\,s^{-1}$, $B = 0.03\,K^{-6.55}\,s^{-1}$, $n = 6.55$, $\tau_o = 2.163 \times 10^{-8}$ s and $U_{eff}/k_B = 65.09$ K for **1**. The U_{eff} of Orbach process is always much lower than the energy difference between the two doublets from HF-EPR probably due to the prominence of anharmonic phonons [52–54].

$$\tau^{-1} = AT + BT^n + \tau_0^{-1} \exp\left(\frac{-U_{eff}}{k_B T}\right) \quad (2)$$

As shown in Fig. S5, comparing the out-of-phase (χ_M") *vs.* frequency curves of **1** and **2** under different magnetic fields, we found that the peak frequency of **1** is at low frequency under the optimal field. The peak value of **2** could not be observed when the frequency is 1000 Hz, implying that the peak appears at a higher frequency. This phenomenon indicates that the relaxation time of **1** is the longer than that of **2**. Comparing the structures of **1** and **2**, we can find that the bond lengths and bond angles of both complexes and the coordination mode of N_3^- anion are nearly the same. The only difference between them is that the structure of **1** is 1D, and that of **2** is 3D. In other words, the structure of **2** is more rigid than that of **1**. Interestingly, we can find that the χ_M" of **1** shows obvious peaks at low applied field and low frequency. However, in **2**, there is no peak in the χ_M" even at the applied magnetic field of 3.0 kOe and the frequency of 1000 Hz. This experiment result indicates that the rigidity has a great influence on the slow relaxation process of the SIMs systems, which also consistent with other works [27,28].

In conclusion, we have synthesized two complexes with the same building unit ($Co(dps)_4(N_3)_2$), but their structures are different. The dps ligand bridges between Co^{II} ions to form a 1D chain with weak interchain interaction in **1**, while a 3D network in **2**. Complex **1** shows the obvious slow relaxation of magnetization in low frequency, but **2** does not. The magnetic fields dependence of far-IR spectra indicate that the structural rigidity has a great influence on the slow relaxation process of the SIMs systems. These results give the direct experimental evidence that spin-phonon coupling plays an important role to regulate the relaxation process, especially in the weak coupling system or SIMs. Our findings are

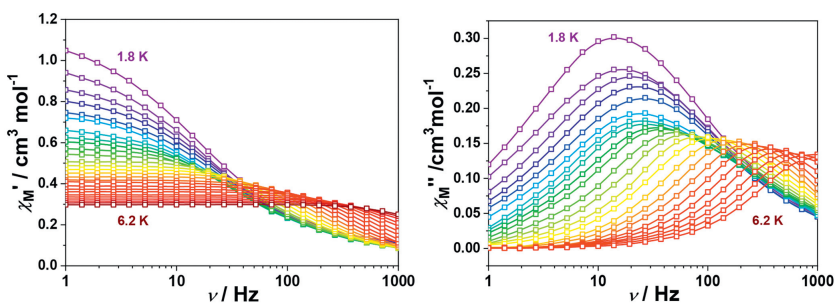

Fig. 6. Frequency-dependent χ_M' (left) and χ_M" (right) AC susceptibilities in $H_{dc} = 1.5$ kOe for **1**.

helpful to guide the design and synthesis of SIMs with high effective energy barrier and blocking temperature.

Declaration of competing interest

We declare that they have no known competing financial interests or personal relationships that could have appeared to influence the work reported in this paper.

Acknowledgments

This work was supported by the National Key Research and Development Program of China (No. 2021YFA1600304), Joint Fund for Regional Innovation and Development (No. U20A2073), National Natural Science Foundation of China (Nos. 22373048, 21973038, 61904119 and 22105089), Jiangxi Provincial Key Laboratory of Functional Molecular Materials Chemistry (No. 20212BCD42018), US National Science Foundation (NSF, No. CHE-2055499), and the Interdisciplinary program of Wuhan National High Magnetic Field Center (No. WHMFC202133). Part of this work was performed at the National High Magnetic Field Laboratory which is supported by NSF Cooperative Agreement No. DMR-1644779 and the State of Florida. P. Tin thanks a Shull Wollan Center Graduate Research Fellowship. A.T. Hand acknowledges the support of the NSF Research Traineeship Program (No. DGE-2152168).

Supplementary materials

Supplementary material associated with this article can be found, in the online version, at doi:10.1016/j.cclet.2024.109600.

References

[1] W. Wernsdorfer, R. Sessoli, Science 284 (1999) 133.
[2] R. Sessoli, D. Gatteschi, A. Caneschi, M.A. Novak, Nature 365 (1993) 141.
[3] M.L. Kirk, D.A. Shultz, D.E. Stasiw, et al., J. Am. Chem. Soc. 135 (2013) 14713–14725.
[4] D.N. Woodruff, R.E.P. Winpenny, R.A. Layfield, Chem. Rev. 113 (2013) 5110–5148.
[5] A.J. Heinrich, W.D. Oliver, L.M.K. Vandersypen, et al., Nat. Nanotechnol. 16 (2021) 1318–1329.
[6] T. Yamabayashi, M. Atzori, L. Tesi, et al., J. Am. Chem. Soc. 140 (2018) 12090–12101.
[7] Q.C. Luo, N. Ge, Y.Q. Zhai, et al., Chin. Chem. Lett. 34 (2023) 107547.
[8] S. Li, Z.Z. Weng, L.P. Jiang, et al., Chin. Chem. Lett. 34 (2023) 107251.
[9] Y. Jiao, Y. Li, Y. Zhou, et al., Chin. Chem. Lett. 34 (2023) 109082.
[10] S. Yu, Z. Chen, H. Hu, et al., Dalton Trans. 48 (2019) 16679–16686.
[11] Z. Chen, S. Yu, R. Wang, et al., Dalton Trans. 48 (2019) 6627–6637.
[12] Z.B. Hu, Z.Y. Jing, M.M. Li, et al., Inorg. Chem. 57 (2018) 10761–10767.
[13] Z.B. Hu, X. Feng, J. Li, et al., Dalton Trans. 49 (2020) 2159–2167.
[14] J.L. Liu, Y.C. Chen, M.L. Tong, Chem. Soc. Rev. 47 (2018) 2431–2453.
[15] M. Briganti, E. Lucaccini, L. Chelazzi, et al., J. Am. Chem. Soc. 143 (2021) 8108–8115.
[16] M. Feng, M.L. Tong, Chem. Eur. J. 24 (2018) 7574–7594.
[17] Y.S. Meng, S.D. Jiang, B.W. Wang, S. Gao, Acc. Chem. Res. 49 (2016) 2381–2389.
[18] C.A. Gould, K.R. McClain, D. Reta, et al., Science 375 (2022) 198–202.
[19] F.S. Guo, B.M. Day, Y.C. Chen, et al., Science 362 (2018) 1400–1403.
[20] Y.S. Ding, N.F. Chilton, R.E.P. Winpenny, Y.Z. Zheng, Angew. Chem. Int. Ed. 55 (2016) 16071–16074.
[21] L. Zhu, Y. Dong, B. Yin, P. Ma, D. Li, Dalton Trans. 50 (2021) 12607–12618.
[22] J. Wang, Q.W. Li, S.G. Wu, et al., Angew. Chem. Int. Ed. 60 (2021) 5299–5306.
[23] S.K. Gupta, R. Murugavel, Chem. Commun. 54 (2018) 3685–3696.
[24] M. He, F.S. Guo, J. Tang, A. Mansikkamäki, R.A. Layfield, Chem. Commun. 57 (2021) 6396–6399.
[25] M. He, F.S. Guo, J. Tang, A. Mansikkamäki, R.A. Layfield, Chem. Sci. 11 (2020) 5745–5752.
[26] J.P. Durrant, J. Tang, A. Mansikkamäki, R.A. Layfield, Chem. Commun. 56 (2020) 4708–4711.
[27] M. Briganti, F. Santanni, L. Tesi, et al., J. Am. Chem. Soc. 143 (2021) 13633–13645.
[28] A. Lunghi, F. Totti, R. Sessoli, S. Sanvito, Nat. Commun. 8 (2017) 14620.
[29] J. Li, S. J Xiong, C. Li, et al., CCS Chem. 2 (2020) 2548–2556.
[30] Q. Chen, F. Ma, Y.S. Meng, et al., Inorg. Chem. 55 (2016) 12904–12911.
[31] Q. Chen, J. Li, Y.S. Meng, et al., Inorg. Chem. 55 (2016) 7980–7987.
[32] Q. Chen, Y.S. Meng, Y.Q. Zhang, et al., Chem. Commun. 50 (2014) 10434–10437.
[33] C. Li, J. Sun, M. Yang, et al., Cryst. Growth Des. 16 (2016) 7155–7162.
[34] Y. Rechkemmer, F.D. Breitgoff, M. van der Meer, et al., Nat. Comm. 7 (2016) 10467.
[35] D.H. Moseley, S.E. Stavretis, K. Thirunavukkuarasu, et al., Nat. Comm. 9 (2018) 2572.
[36] D.H. Moseley, S.E. Stavretis, Z. Zhu, et al., Inorg. Chem. 59 (2020) 5218–5230.
[37] A.N. Bone, C.N. Widener, D.H. Moseley, et al., Chem. Eur. J. 27 (2021) 11110–11125.
[38] J.G.C. Kragskow, J. Marbey, C.D. Buch, et al., Nat. Comm. 13 (2022) 825.
[39] D.H. Moseley, Z. Liu, A.N. Bone, et al., Inorg. Chem. 61 (2022) 17123–17136.
[40] F. Liedy, J. Eng, R. McNab, et al., Nat. Chem. 12 (2020) 452–458.
[41] X.Z. Luo, S. Xin, J.H. Yu, J Chin, Inorg. Chem. 26 (2010) 1299–1302.
[42] N.F. Chilton, R.P. Anderson, L.D. Turner, A. Soncini, K.S. Murray, J. Comput. Chem. 34 (2013) 1164–1175.
[43] The SPIN program was developed by Dr. Andrzej Ozarowski to "simulates powder or single-crystal EPR spectra for spin states with ½ < S < 5." It is free at https://nationalmaglab.org/user-facilities/emr/software/.
[44] L. Chen, J. Wang, J.M. Wei, et al., J. Am. Chem. Soc. 136 (2014) 12213–12216.
[45] A.N. Bone, S.E. Stavretis, J. Krzystek, et al., Polyhedron 184 (2020) 114488.
[46] C.N. Widener, A.N. Bone, M. Ozerov, et al., Chin. J. Inorg. Chem. 35 (2020) 1149–1156.
[47] S.E. Stavretis, D.H. Moseley, F. Fei, et al., Chem. Eur. J. 25 (2019) 15846–15857.
[48] P. Tin, S.E. Stavretis, M. Ozerov, et al., Appl. Mang. Reson. 51 (2020) 1411–1432.
[49] J. Vallejo, M. Viciano-Chumillas, F. Lloret, et al., Inorg. Chem. 58 (2019) 15726–15740.
[50] P. Tin, A.N. Bone, N.N. Bui, et al., J. Phys. Chem. B 126 (2022) 13268–13283.
[51] Y.N. Guo, G.F. Xu, Y. Guo, J. Tang, Dalton Trans. 40 (2011) 9953–9963.
[52] A. Albino, S. Benci, L. Tesi, et al., Inorg. Chem. 58 (2019) 10260–10268.
[53] F. Santanni, A. Albino, M. Atzori, et al., Inorg. Chem. 60 (2021) 140–151.
[54] A. Lunghi, S. Sanvito, J. Chem. Phys. 153 (2020) 174113.